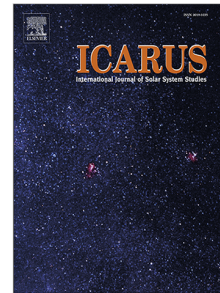# Journal Pre-proof

Limited recharge of the southern highlands aquifer on early Mars

Eric Hiatt, Mohammad Afzal Shadab, Sean P.S. Gulick, Timothy A. Goudge, Marc A. Hesse

Please cite this article as: E. Hiatt, M.A. Shadab, S.P.S. Gulick et al., Limited recharge of the southern highlands aquifer on early Mars. *Icarus* (2023), doi: https://doi.org/10.1016/j.icarus.2023.115774.

This is a PDF file of an article that has undergone enhancements after acceptance, such as the addition of a cover page and metadata, and formatting for readability, but it is not yet the definitive version of record. This version will undergo additional copyediting, typesetting and review before it is published in its final form, but we are providing this version to give early visibility of the article. Please note that, during the production process, errors may be discovered which could affect the content, and all legal disclaimers that apply to the journal pertain.

Highlights

Highlights

Limited Recharge of the Southern Highlands Aquifer on Early Mars

Eric Hiatt,Mohammad Afzal Shadab,Sean P.S. Gulick,Timothy A. Goudge,Marc A. Hesse

- Analytic and numerical solutions for an unconfined aquifer beneath Mars' southern highlands provides first-order estimates of groundwater table elevation.

- The key control on the steady groundwater table elevation is the ratio between mean recharge and mean hydraulic conductivity of the aquifer.

- For commonly assumed values of hydraulic conductivity, the steady recharge must be at the lower end of the estimated range of recharge fluxes.

Limited Recharge of the Southern Highlands Aquifer on Early Mars

Eric Hiatt[a,b,c,*], Mohammad Afzal Shadab[b,c,d], Sean P.S. Gulick[a,b,c], Timothy A. Goudge[a,c,e] and Marc A. Hesse[a,d]

[a]Department of Geological Sciences Jackson School of Geosciences The University of Texas at Austin

[b]University of Texas Institute for Geophysics The University of Texas at Austin

[c]Center for Planetary Systems Habitability The University of Texas at Austin

[d]Oden Institute for Computational Engineering and Sciences The University of Texas at Austin

[e]CIFAR Azrieli Global Scholars Program CIFAR Toronto Ontario Canada

ARTICLE INFO

ABSTRACT

To determine plausible groundwater recharge fluxes on early Mars, we developed analytic and numerical solutions for an unconfined steady-state aquifer beneath the southern highlands. We showed that the aquifer's mean hydraulic conductivity, K, is the primary constraint on the plausible magnitude of the mean steady recharge, r. By using geologic constraints, a mean hydraulic conductivity of $K \sim 10^{-7}$ m/s, and varying shoreline elevations and recharge distributions, the mean recharge must be of the order of 10^{-2} mm/yr. Recharge for other values of K can be estimated as $r \sim 10^{-5} K$. Our recharge value is near the low end of previous estimates and significantly below published precipitation estimates. This suggests that, in a steady hydrologic cycle, most precipitation forms runoff as opposed to infiltrating into the subsurface. Alternatively, high rates of runoff production combined with a sufficiently slow transient aquifer response to recharge may limit major groundwater upwelling prior to the cessation of climatic excursions causing precipitation.

1. Introduction

The surface of Mars retains several planetary scale structures. The largest is the crustal dichotomy separating Mars' northern lowlands from its southern highlands via an abrupt ~ 5 km topographic transition (Figure 1). In stark contrast to the smooth plains in the north, the highlands preserve the oldest, most heavily cratered terrain on the planet as well as two large impact basins, Hellas and Argyre (Smith et al., 1999). These structures formed prior to $\sim$3.7 Ga, in the Noachian Era, when Mars is also hypothesized to have had an active hydrologic cycle (Carr, 1986; Clifford, 1993; Frey, 2008; Werner, 2008). The formation of these structures would have impacted any possible surface and groundwater processes due to their associated topographic lows.

There is ample evidence for liquid water on Mars' surface early in the planet's history. The eroded remains of poorly integrated fluvial drainage systems, called "valley networks", dissect the highlands (Milton, 1973; Goldspiel and Squyres, 1991; Carr, 1996; Hynek and Phillips, 2001). Spectral data strengthen inferences of past surface water related processes with observations of hydrated silicates that suggest near surface aqueous mineral alteration (Mustard et al., 2008; Ehlmann et al., 2009; Carter et al., 2013). Open and closed crater lakes have been identified throughout the Noachian terrain, providing further evidence of standing bodies of water on the Martian surface (Cabrol and Grin, 1999; Fassett and Head III, 2008; Di Achille and Hynek, 2010). Additionally, observations in Argyre and Hellas also support the possible past existence of large standing bodies of water within these basins (Parker et al., 2000; Wilson et al., 2010; Dohm et al., 2015; Hiesinger and Head, 2002; Hargitai et al., 2018; Zhao et al., 2020). Many have also argued that an immense ocean once existed within the lowlands (e.g., Parker et al., 1989, 1993; Carr and Head, 2003).

Evidence of surface water processes and standing bodies of water naturally leads to questions regarding the formation and extent of any groundwater systems. A globally connected groundwater system has been inferred in numerous geomorphic and numerical modeling based studies (e.g., Clifford, 1993; Andrews-Hanna et al., 2007; Di Achille and Hynek, 2010; Salese et al., 2019). Additionally, observations of layered deposits in Arabia Terra (Figure 1) have been interpreted as evaporites resulting from groundwater upwelling (Christensen et al., 2000; Golombek et al., 2003; Squyres et al., 2004; McLennan et al., 2005; Grotzinger et al., 2005; Bibring et al., 2007;

*Corresponding author

✉ eric.hiatt@utexas.edu (E. Hiatt); mashadab@utexas.edu (M.A. Shadab)

ORCID(s): 0000-0003-1087-007X (E. Hiatt); 0000-0002-0797-5017 (M.A. Shadab); 0000-0002-2532-3274 (M.A. Hesse)

Limited Recharge of the Southern Highlands Aquifer on Early Mars

Andrews-Hanna et al., 2007). These findings suggest that Mars had an active groundwater hydrology, but its coupling with surface hydrology through groundwater recharge and upwelling is poorly understood.

Here we investigate the plausible values of groundwater recharge as constrained by large-scale topography and geologic observations. The aim of this work is not to constrain the specific hydrology at discrete time periods on early Mars, but to establish constraints on the total rates of groundwater recharge that are plausible given geologic observations. With this aim, we then compare our findings to published estimates of precipitation rates. In doing so, some insight into groundwater-to-surface water coupling may be gained, however this requires simplifying assumptions regarding basin hydraulic head levels, hydraulic conductivity, and recharge distributions.

To examine the effect of standing bodies of water on possible groundwater recharge, we use mean shoreline elevations of Deuteronilus (-3790 m), Arabia (-2090 m), and Meridiani (0 m) as illustrative examples (see Table 1 in Carr and Head (2003) and Figure 1). The existence of a northern ocean remains contentious, with some studies arguing that the kilometer-scale deviation of equipotential shorelines preclude the possibility of any ocean(s) (e.g., Malin and Edgett, 1999; Sholes et al., 2019, 2021; Sholes and Rivera-Hernández, 2022); however, others have suggested that true polar wander and/or deformation associated with the Tharsis Rise can explain these discrepancies (Perron et al., 2007; Citron et al., 2018; Chan et al., 2018). Although each of these individual shorelines is uncertain, together they allow hydrologic models to span a large parameter space in Mars' total water budget. Here, we show that the existence of a northern ocean, regardless of extent, is a secondary control on groundwater when compared to the geometry of the dichotomy.
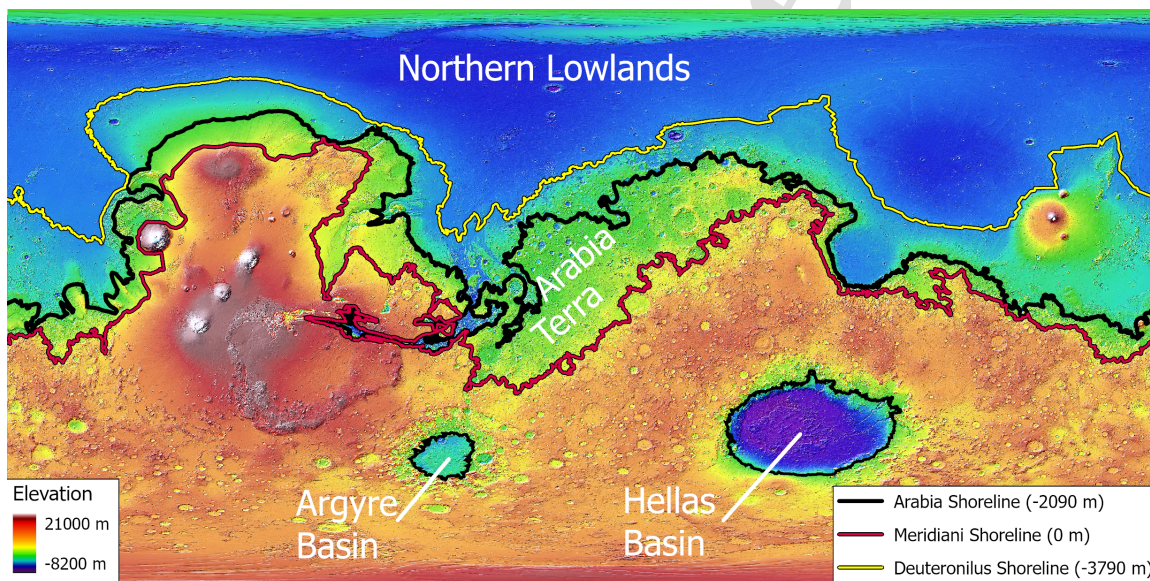

Figure 1: Topography of Mars derived from Mars Orbiter Laser Altimeter (MOLA) aboard the Mars Global Surveyor (MGS) mission (Smith et al., 1999). Hellas and Argyre impact basins are labeled along with the northern lowlands. Three mean shoreline elevations are taken from Parker et al. (1989) and Carr and Head (2003). Argyre and Hellas impact basins are outlined at an elevation of -2090 m.

The distribution of valley networks offers insight into groundwater table elevation, which often sets the local base level to which fluvial systems can erode. The wide distribution of incised valley networks implies that any groundwater table was likely below the surface topography over much of the planet (Hynek et al., 2010). Similarly, Arabia Terra's noticeable lack of incised valley networks and the presence of inverted fluvial channels suggests that the region was a depositional environment, with a groundwater table at or near the surface consistent with rover observations (Squyres et al., 2004; Grotzinger et al., 2005; Davis et al., 2016, 2019). Evidence that the groundwater table was significantly below topography, everywhere except in Arabia Terra, provides a constraint on plausible groundwater recharge fluxes.

Published aquifer recharge and precipitation rates vary by orders of magnitude. Estimates of water availability due to snow and ice accumulation give values ranging from 10^{-2} to 10^{3} mm/yr (e.g., Wordsworth et al., 2015; Fastook and Head, 2015; von Paris et al., 2015) and estimates of precipitation range of $10^{0} - 10^{3}$ mm/yr (e.g., Kamada et al.,

2020; Wordsworth et al., 2015). Geomorphic studies have estimated water associated with runoff production between 10^2 to 10^5 mm/yr (Ramirez et al., 2020; Hoke et al., 2011). However, these studies only provide an upper bound on groundwater recharge due to the unknown partitioning between runoff and infiltration.

Direct estimates of recharge from previous modeling studies vary between 10^{-2} to 10^3 mm/yr, but require the specification of unknown aquifer properties (Harrison and Grimm, 2009; Andrews-Hanna et al., 2007, 2010; Luo et al., 2011; Horvath and Andrews-Hanna, 2017). Here, we examine the importance of these properties individually, the effects of possible standing bodies of water, and consequences associated with varying recharge distributions on the aquifer using novel analytic and numerical groundwater models. By comparing solutions with the inferred depositional environment within Arabia Terra and the distribution of valley networks, we ask: what are plausible mean recharge estimates for a steady-state aquifer on early Mars?

2. Methodology

2.1. Model for the southern highlands aquifer

Similar to many previous large-scale groundwater studies on Mars (e.g., Clifford, 1993; Hanna and Phillips, 2005; Luo and Howard, 2008), we use the Dupuit-Boussinesq model (Dupuit, 1863; Forchheimer, 1901; Boussinesq, 1903). This approach relies on the large aspect ratio of the aquifer to assume groundwater flows predominantly horizontal. This assumption reduces the dimensionality and computational cost of the model, which makes planetary-scale computations feasible. For a recent review of this approach to large-scale groundwater modeling, with a derivation of the governing equations and an explanation of their physical interpretation, see Troch et al. (2013). At steady state, this model leads to the following non-linear elliptic partial differential equation for the height, h, of the groundwater table above the base of the aquifer given by

$$-\nabla \cdot [K\, h \nabla h] = r\, \chi(\theta, \theta_r), \tag{1}$$

where θ is the angle from the south pole or southern colatitude, K is the hydraulic conductivity, r is the recharge, and χ is an indicator function. The divergence and gradient take their standard form in spherical shell coordinates; see SI Section S3.2. For clarity of presentation, we assume that both K and r are constant and hence refer to them as the mean hydraulic conductivity and the mean recharge; however, our numerical computations can be extended to spatially variable conductivity and recharge. Figure 2a shows that the base of the aquifer is assumed to be at an elevation of $z_B = -9$ km, consistent with previous studies (Andrews-Hanna et al., 2010; Andrews-Hanna and Lewis, 2011). For a mean elevation of the highlands of $z_H = 1$ km, the aquifer has a maximum thickness of $d = z_H - z_B = 10$ km, similar to previous work (Hanna and Phillips, 2005). In this reference frame, the elevation of the groundwater table is given by $z_{GW} = z_B + h$.

We assume that the recharge, r, is evenly distributed in a latitudinal band of angular width, $\Delta\theta_r = 180° - 2\theta_r$, between the colatitude θ_r and $180° - \theta_r$ (Figure 2b). This band is defined by the indicator function $\chi(\theta, \theta_r)$ that is one for $\theta_r \leq \theta \leq 180° - \theta_r$ and zero otherwise. We note that the recharge, r, is a *flux*, i.e., a volume per unit area per unit time. The total *rate* of recharge can be obtained by integrating the flux over the surface area of the aquifer. We assume that groundwater recharge occurs only on land, so that the boundaries of the recharge band may be influenced by the shorelines. This implies that for the same recharge flux, r, and width of recharge band, $\Delta\theta_r$, the total aquifer recharge rate changes for different shore lines. Finally, the recharge should be considered as a temporally averaged quantity, because we consider a steady system.

2.2. Analytic Solutions for an idealized spherical cap aquifer

To gain a first-order understanding of the groundwater dynamics, we derive analytic solutions in an idealized spherical cap aquifer with azimuthal symmetry. The spherical caps corresponding to the three shorelines shown in Figure 1 are illustrated in Figure 2c-e. We choose the southern colatitude of the mean shoreline, θ_o, so that the surface area of the idealized spherical cap aquifer is equivalent to the area enclosed by the complex shoreline in Figure 1. In this limit, the solution is only a function of latitude, θ and equation (1) reduces to the following differential equation

$$-\frac{1}{R\sin\theta}\frac{d}{d\theta}\left[\frac{K}{R}\sin\theta\, h\frac{dh}{d\theta}\right] = r\,\chi(\theta, \theta_r) \quad \text{on} \quad \theta \in \left[0, \theta_o\right], \tag{2}$$

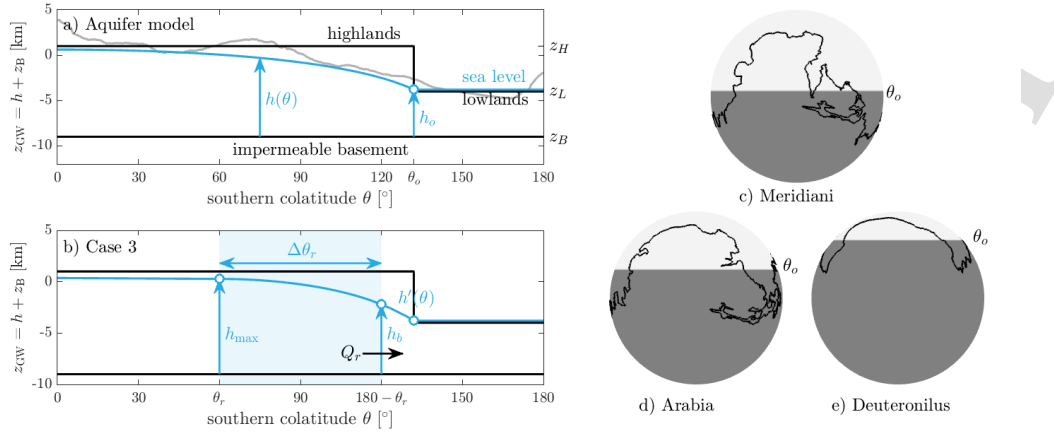Limited Recharge of the Southern Highlands Aquifer on Early Mars

Figure 2: Simplified model and analytic solutions. *a)* Cross-section through the one-dimensional azimuthally symmetric Dupuit-Boussinesq model for the southern highlands aquifer. The azimuthally averaged MOLA topography is shown in gray and the simplified step function topography for the Deuteronilus shoreline is shown in black. The groundwater table and sea level are shown in blue. *b)* Construction of the composite solution with a longitudinal recharge band for case 3. *c-e)* Three shorelines from Carr and Head (2003) shown in black together with the equal-area spherical cap aquifer shown in dark gray and the complementary spherical cap ocean in light gray.

where $R \approx 3390$ km is the mean radius of Mars (Smith et al., 1999), and θ_{o} is the southern colatitude of the mean shoreline of the northern ocean and r is the mean recharge flux. We assumed a simple step in topography at the shoreline, θ_{o}, between the mean elevation of the highlands, $z_{\mathrm{H}} = 1$ km, and the mean elevation of the lowlands, $z_{\mathrm{L}} = -4$ km (Figure 2*d*). At the south pole, the groundwater table is horizontal by symmetry, $dh/d\theta|_{\theta=0} = 0$, and along the shoreline the head is prescribed, $h(\theta_{\mathrm{o}}) = h_o$ (Figure 2a).

In particular, we are interested in the effect that the width of the recharge band, $\Delta\theta_r$, has on the groundwater table and plausible recharge fluxes. As the width of the latitudinal recharge band, $\Delta\theta_r$, is varied, three different cases must be distinguished in the analytical solution. The first and simplest case is uniform recharge over the entire aquifer, and the other two cases are for partial recharge.

2.2.1. Uniform recharge (Case 1)

In the simplest case, the recharge is uniform across the entire highlands, $\theta_r = 0$ and $\chi(\theta, 0) = 1$. We have presented the analytic solutions for this limiting case in (Shadab et al., 2022). The head is given by

$$h(\theta) = \sqrt{h_o^2 + 2\frac{rR^2}{K} \ln\left|\frac{\cos\theta + 1}{\cos\theta_{\mathrm{o}} + 1}\right|}, \quad \text{for} \quad \theta \in [0, \theta_{\mathrm{o}}], \tag{3}$$

and shown in Figure 2*a*. The solution for case 1 becomes the basis for the analytic solutions with heterogeneous recharge distributions discussed below. Shadab et al. (2022) also shows the associated specific discharge, $q(\theta) = -K dh/d\theta$, and the discharge $Q(\theta) = h(\theta)l(\theta)q(\theta)$, where $l = 2\pi R \sin\theta$ is the length of the small circle with colatitude θ. Mass/volume balance at steady state requires that the discharge must equal the recharge rate, $Q(\theta) = rA(\theta)$, where $A(\theta) = 2\pi R^2 (1 - \cos\theta)$ is the area of the spherical cap. These relations also hold for the other cases given below.

2.2.2. Partial recharge

Here, we present new solutions for an unconfined aquifer with partial recharge, $0 < \theta_r < 90°$. In all cases, we assume recharge in a longitudinal band between θ_r and $180° - \theta_r$ of width $\Delta\theta_r = 180° - 2\theta_r$. First, we consider the case where the northern boundary of the precipitation band, $180° - \theta_r$, is north of the dichotomy shoreline, θ_{o}, that bounds the aquifer (Case 2). Then, we consider the case of a latitudinal precipitation band that is entirely south of the dichotomy shoreline (Case 3). In this latter case, the northern-most part of the aquifer does not receive recharge and flow in this regions is entirely due to lateral inflow from the south.

- **Case 2** ($180° - \theta_r \geq \theta_o$): In this case, recharge starts at the most southern colatitude of the recharge band, θ_r, and extends to our chosen ocean shoreline at θ_o. The solution for the head is piece-wise defined and given by

$$h(\theta) = \begin{cases} h_{\max} = h(\theta_r) = \text{const.}, & 0 \leq \theta < \theta_r, \\ \\ \sqrt{h_o^2 + 2\dfrac{rR^2}{K}\Delta(\theta, \theta_r, \theta_o)}, & \theta_r \leq \theta \leq \theta_o, \end{cases} \tag{4}$$

where we have introduced the geometric function

$$\Delta(\theta, \theta_r, \theta_o) = \ln\left|\frac{\sin\theta}{\sin\theta_o}\right| - \cos\theta_r \ln\left|\frac{(\cos\theta + 1)\sin\theta_o}{(\cos\theta_o + 1)\sin\theta}\right| \tag{5}$$

that arises from the integration on the sphere. In the limit of $\theta_r \to 0$ this function reduces the logarithmic term in equation 3.

- **Case 3** ($180° - \theta_r < \theta_o$): In this case, recharge starts at θ_r and extends only until $180° - \theta_r < \theta_o$, so that the northern most portion of the aquifer does not receive any recharge, $r = 0$, but a discharge, Q_r, from the region within the latitudinal recharge band. The different elements in the construction of this solution are illustrated in Figure 2b. The solution for the head in the region without a recharge is given by

$$h'(\theta) = \sqrt{h_o^2 + \frac{Q_r}{\pi K}\ln\left|\frac{\tan(\theta_o/2)}{\tan(\theta/2)}\right|}. \tag{6}$$

The discharge this area receives is the total recharge integrated over the latitudinal recharge band and given by $Q_r = 2\pi R^2\left(\cos(\theta_r) - \cos(180° - \theta_r)\right)r$. Given Q_r, the head at the northern boundary of the latitudinal recharge band can be calculated as

$$h_b = h'(180° - \theta_r) = \sqrt{h_o^2 + \frac{Q_r}{\pi K}\ln\left|\frac{\tan(\theta_o/2)}{\tan((180° - \theta_r)/2)}\right|}. \tag{7}$$

This head forms the boundary condition for the solution within the latitudinal recharge band, which is similar to equation (4) except that h_o is replaced with h_b. The full piece-wise solution for case 3 is then given by

$$h(\theta) = \begin{cases} h_{\max} = h(\theta_r) = \text{const.}, & 0 \leq \theta < \theta_r, \\ \\ \sqrt{h_b^2 + 2\dfrac{rR^2}{K}\Delta(\theta, \theta_r, 180° - \theta_r)}, & \theta_r \leq \theta < 180° - \theta_r, \\ \\ h'(\theta) = \sqrt{h_o^2 + \dfrac{Q_r}{\pi K}\ln\left|\dfrac{\tan(\theta_o/2)}{\tan(\theta/2)}\right|}, & 180° - \theta_r \leq \theta \leq \theta_o, \end{cases} \tag{8}$$

where $\Delta(\theta, \theta_r, 180° - \theta_r)$ is given by equation (5).

The solutions for all three cases, equations (3), (4) and (8), depend only on the dimensionless ratio r/K and not on r and K individually. The physical interpretation of this ratio is that it takes more recharge to sustain the water table at a given height if the regolith is very conductive and allows the water to flow away quickly. Therefore, below we will discuss the plausible recharge values in terms of this ratio.

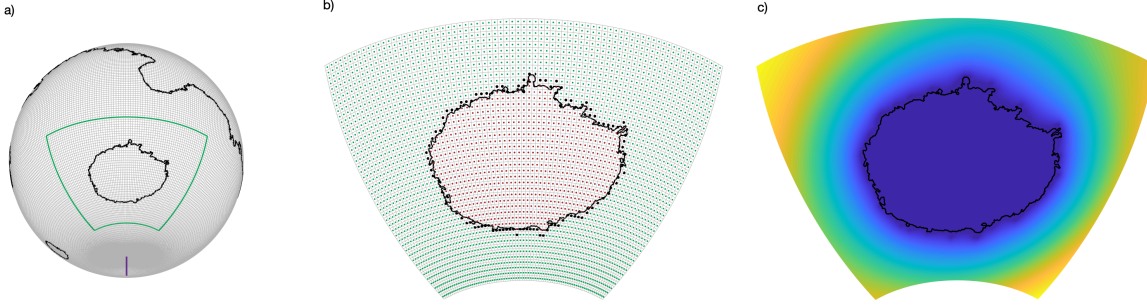Limited Recharge of the Southern Highlands Aquifer on Early Mars

Figure 3: Treatment of complex shorelines in the numerical groundwater model. *a*) The global mesh is shown in gray with the Arabia shoreline and the equivalent elevation shorelines in the Hellas and Argyre basins are shown in black. The green outline shows the zoom-in area shown in panels *b* and *c*. *b*) Numerical mesh in the vicinity of the Hellas basin. Active cells are shown by green dots, and inactive cells are shown by red dots. Black dots identify the cells where the boundary condition corresponding to the Hellas shoreline is imposed. *c*) The resulting numerical solution for the groundwater table in the vicinity of the shoreline in the Hellas basin.

2.3. Maximum recharge value

The analytic solutions presented above allow a first-order estimate of the plausible r/K ratio over a wide parameter space. To place constraints on plausible recharge values, we used the observation that the groundwater table was below topography in the majority of the highlands. In our analytic model widespread upwelling would occur if the elevation of the groundwater table exceeds the mean elevation of the highlands, $\max(z_{GW}) = z_H$, see Figure 2*b*. Because the water table is always highest at the south pole this is equivalent to requiring that $h(0) = z_H - z_B = d$. Substituting this into equations (3), (4), (8) and solving for r/K, we obtain the maximum r/K ratio for each case as

$$
\left.\frac{r}{K}\right|_{\max} = \begin{cases} \dfrac{d^2 - h_o^2}{2R^2 \ln\left|\frac{\cos\theta + 1}{\cos\theta_o + 1}\right|}, & \text{case 1,} \\[3ex] \dfrac{d^2 - h_o^2}{2R^2 \Delta(\theta_r, \theta_r, \theta_o)}, & \text{case 2,} \\[3ex] \dfrac{d^2 - h_o^2}{A_s/\pi \ln\left(\frac{\tan(\theta_o/2)}{\tan(180° - \theta_r)/2}\right) + 2R^2\Delta(\theta_r, \theta_r, 180° - \theta_r)}, & \text{case 3.} \end{cases}
\tag{9}
$$

These results will be discussed in section 3.

2.4. Numerical Model for southern highlands aquifer

To investigate the effects of complex shorelines and basins on plausible recharge fluxes, we developed a numerical model for the highlands' aquifer. We non-dimensionalized equation (1) and discretized it in spherical shell geometry. The model uses conservative finite differences on a tensor product grid with an operator-based implementation (LeVeque, 1992). The resulting non-linear system of equations is solved with the Newton-Raphson method. More details of the numerical model and the benchmark test can be found in SI Section S3. For consistency between the analytic and numerical models all dimensional simulation results use a hydraulic conductivity of, $K = 10^{-7}$ m/s.

To obtain the locations of the shorelines in the northern lowlands and basins, the MOLA topography is down-sampled to our grid pixel resolution of 1.2° (Figure 3*a*). Next, these shorelines are used to divide the computational domain into the highlands aquifer and three open water basins by assuming an equipotential surface across a standing body of water. Cells within these basins must be excluded from the computations (Figure 3*b*). We locate the cell faces corresponding to the elevation of the chosen basin, for example the cells marked red within the Hellas basin in

189 Figure 3*b*. The entries corresponding to inactive cells can be removed from the matrix equation using the projection
190 approach (see Shadab and Hesse, 2022, for details). The reduced matrix system of discrete governing equations can
191 then be solved on the active cells (green dots in Figure 3*b*). The resulting head distribution in the vicinity of the Hellas
192 basin is shown in Figure 3*c*.

193   When a portion of the specified recharge band extends north of the chosen shoreline, the prescribed recharge flux
194 is not added to the system under the assumption that rainfall in a large body of water has a net zero effect on the water
195 level. As such, the same latitudinal recharge band can lead to different total recharge rates for different shorelines.

3. Results

197   The analytic and numerical aquifer models provide complementary information about the plausible steady-state
198 recharge values for Mars' highlands aquifer. The analytic solution gives insight into the relationship between recharge
199 and hydraulic conductivity, whereas the numerical results allow us to investigate the effects of complex shoreline
200 geometries. Although the analytic solution is highly simplified, the order of magnitude agreement between both
201 solutions provides confidence between the solutions.

202   Neither the mean hydraulic conductivity nor the mean recharge of the highlands aquifer are known. Our analysis
203 shows that the solution for the head, given by equations (3, 4, 8), is primarily a function of the dimensionless ratio
204 between recharge and hydraulic conductivity, r/K. This ratio allows us to estimate which recharge values are plausible
205 given any proposed mean hydraulic conductivity. For example, Figures 4*a*-4*c* show the elevation of the groundwater
206 table in the spherical cap aquifer for different shorelines and increasing recharge values. For a hydraulic conductivity of
207 10^{-7} m/s, the analytic model predicts recharge values on the order of 10^{-2} mm/yr are capable of raising the groundwater
208 table to the surface.

209   Requiring groundwater elevation lower than topography in the majority of the highlands constrains plausible r/K
210 ratios. Figure 4*d* shows the plausible combinations of hydraulic conductivity and recharge for the Arabia shoreline.
211 This illustrates that reducing the mean K by an order of magnitude requires a similar drop in the mean r to prevent
212 widespread upwelling. The effects of varying other parameters, such as the chosen shoreline (Figure 4*a*-4*c*) or the
213 recharge distribution (Figure 4*e*-4*g*) are less than an order magnitude. For example, if the width of the recharge band,
214 $\Delta\theta_r$, is varied by $\pm 20°$ around the preferred value of $90°$ for an aquifer with $K = 10^{-7}$ m/s the maximum plausible
215 values of the mean recharge for the three shorelines vary only between $6 \cdot 10^{-3}$ and $1.6 \cdot 10^{-2}$ mm/yr (Figure 4*h*). The
216 analytic model already demonstrates that the recharge estimates are not very sensitive to the recharge distribution. The
217 numerical results below show that this is even less important when complex shorelines are present. In that case, the
218 hydraulic head level is more sensitive to the distance to the shoreline than it is to the recharge distribution.

219   Analysis of the simplified spherical cap aquifer model demonstrates that the elevation of the groundwater table is
220 primarily a function of the r/K ratio. Although the mean K of the southern highlands is not known, reasonable values
221 in the range of 10^{-6} to 10^{-8} m/s (Hanna and Phillips, 2005) require very low groundwater recharge rates to avoid
222 widespread groundwater upwelling (Figure 4*d*). This conclusion is relatively insensitive to the particular shoreline
223 chosen, the latitudinal width of the precipitation band, or the depth of the aquifer base. The particular value of the
224 ratio r/K is primarily determined by the large surface area of the highlands relative to the cross-sectional area of the
225 aquifer, as discussed in Section 4.

226   To explore the effect of complex shorelines, we present numerical solutions using the Arabia shoreline, $K = 10^{-7}$
227 m/s, and $r = 10^{-2}$ mm/yr (Figure 5). First, we explore the effect of the shoreline alone and then consider the influence
228 of adding the Hellas and Argyre basins. When comparing the analytic solution for the spherical cap aquifer (Figure 5*a*)
229 with the numerical solution for the Arabia shoreline (Figure 5*b*), we observe an overall drop in the elevation of the
230 groundwater table. The complex shoreline generates a local maximum in groundwater elevation at the farthest location
231 from a shoreline within the precipitation band. The complex shoreline has an increased shoreline length and reduces
232 the distance to drain into a basin resulting in more effective drainage. The presence of basins further lowers the head
233 in the aquifer (Figure 5*c*). These basins provide additional shorelines within the highlands that help drain the aquifer.
234 Results for other shorelines are provided in the SI Section S4.3 and S4.4.

235   Overall, our numerical model demonstrates that complex shorelines lower the head in the aquifer and therefore
236 increase the plausible value of mean recharge. However, these geometric effects do not change the order of magnitude of
237 the plausible range for r/K. As such, the unknown mean hydraulic conductivity of the highlands remains the dominant
238 control on the allowable mean recharge. In Figure 6, we explore the location and extent of groundwater upwelling in
239 the highlands as a function of mean recharge in an aquifer bounded by the Arabia shoreline at the dichotomy and

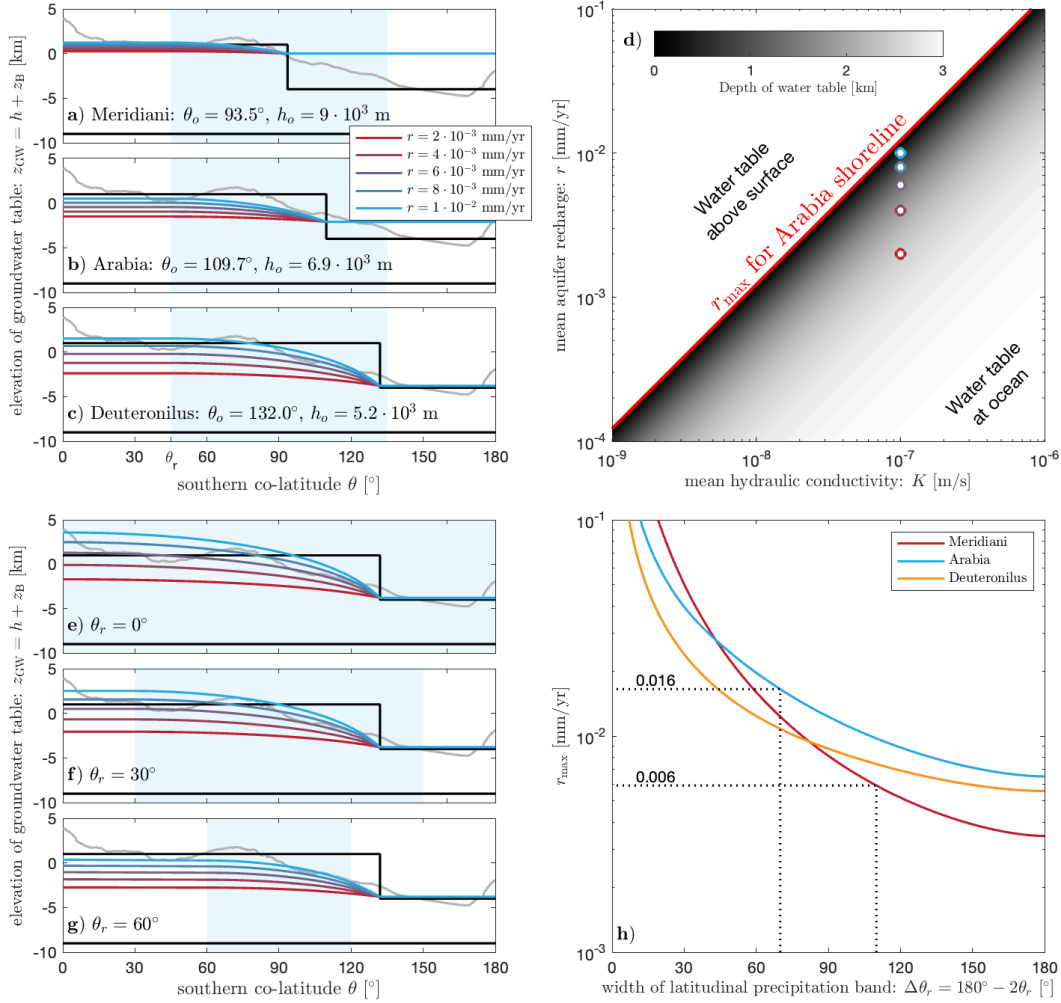Limited Recharge of the Southern Highlands Aquifer on Early Mars

Figure 4: *a-c*) Analytic solution for steady unconfined aquifer on a spherical shell. Elevation of the groundwater table for the mean elevations of the Meridiani, Arabia, and Deuteronilus shorelines of Carr and Head, 2003. In each case, the groundwater table is shown for multiple recharge values, as given by the legend in panel *b*. *d*) Depth of groundwater beneath mean highland elevation, $z_H = 1$ km for the Arabia shoreline. The parameters corresponding to the solutions from panel *b*) are plotted as dots. The maximum plausible recharge from equation (9) is shown in red. Note that these solutions assume that recharge extends to the shoreline, $\theta_o \leq 180° - \theta_r$. *e-g*) The Deuteronilus shoreline is utilized to examine the effect of recharge distribution. The region receiving recharge is varied and shaded in shaded blue. The recharge color scheme, used in *a-c*, remains. *h*) The effect of the thickness of the recharge band on the maximum recharge flux is examined. Note that the hydraulic conductivity remains constant at $K = 10^{-7}$ m/s and the x-axis is the total width of recharge above and below the equator. The gray line in the elevation plots refers to the azimuthally averaged MOLA topography.

shorelines of equivalent elevation in Hellas and Argyre. Figure 6*a*-6*c* shows the depth, compared to topography, of the groundwater table for a succession of simulations with increasing amounts of recharge. Areas with deep blue colors are submerged, whereas areas of groundwater upwelling are shown in white and light blue regions. For $r = 10^{-2}$ mm/yr the highlands do not experience significant upwelling outside of some deep craters (Figure 6*a*), suggesting r is too low. Increasing the recharge to $3 \cdot 10^{-2}$ mm/yr forms a region of groundwater upwelling in Arabia Terra (Figure 6*b*), where geologic observations suggest upwelling has occurred (e.g., McLennan et al., 2005; Grotzinger et al., 2005;

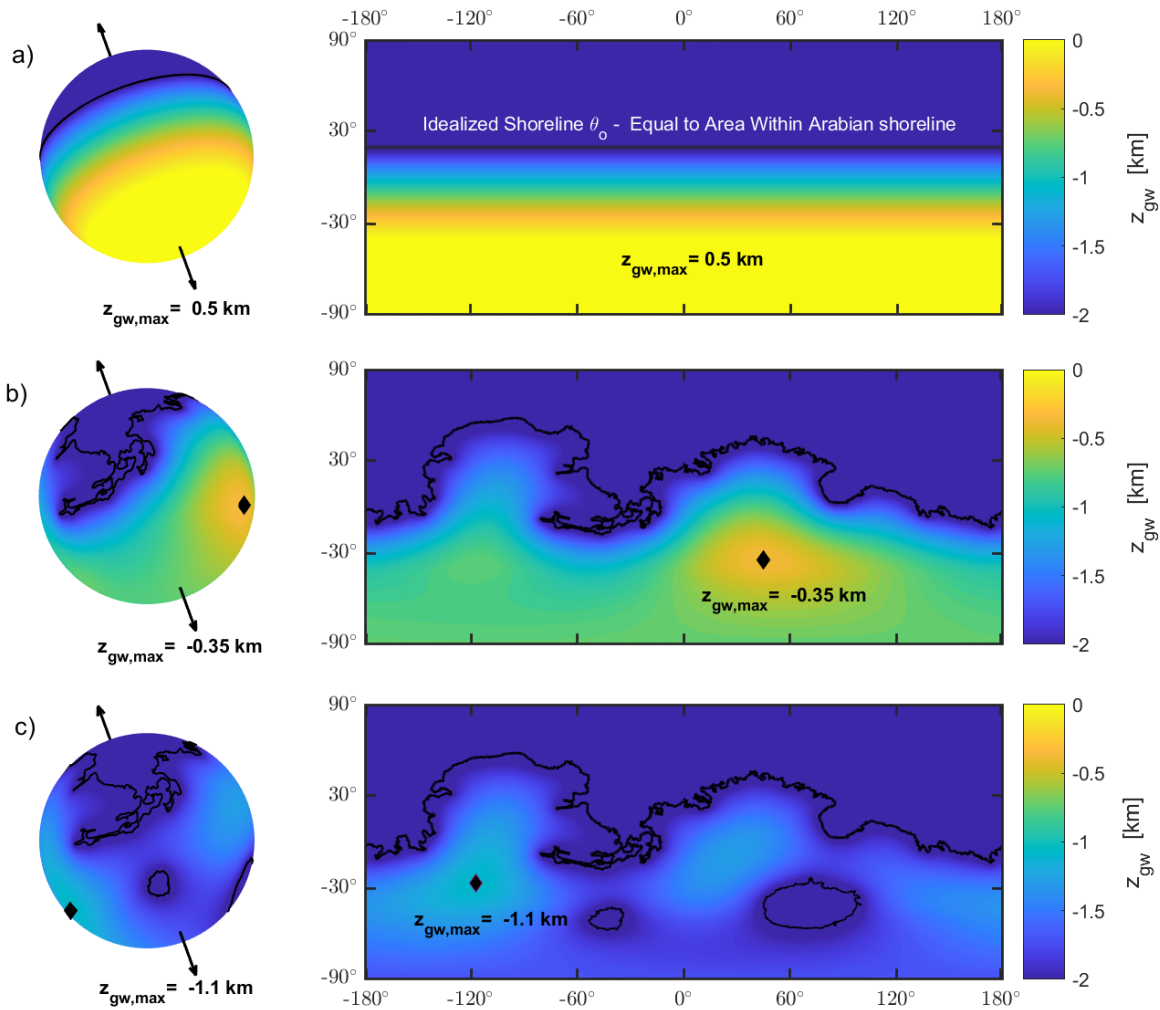Limited Recharge of the Southern Highlands Aquifer on Early Mars

Figure 5: Effect of complex geometry for an aquifer with a recharge flux of 10^{-2} mm/yr evenly distributed between -45° and 45°: *a*) Analytic solution from equation 4 with mean Arabia shoreline. *b*) Numerical solution with Arabia shoreline. *c*) Numerical solution with Arabia shoreline and standing water in Hellas and Argyre basins. The hydraulic head level in the basins is assumed to be equal to the Arabia shoreline elevation. All numerical solutions presented in this work assume a hydraulic conductivity of $K = 10^{-7}$ m/s and assume that all basins have shoreline elevations equivalent to the Arabia Terra shoreline at -2090 m. Results for other shorelines are provided in the SI Section S4.3 and S4.4.

Davis et al., 2016, 2019). A further increase in recharge to only 10^{-1} mm/yr results in large areas of the highlands experiencing upwelling beyond that supported by observations (Figure 6c).

The area of the highlands that experiences groundwater upwelling grows rapidly with increasing recharge (Figure 6d). Therefore, the lack of evidence for pervasive depositional environments in the highlands places a constraint on the plausible r/K ratio. For the mean hydraulic conductivity $K = 10^{-7}$ m/s, the recharge that best reproduces the observed geology qualitatively is approximately $3 \cdot 10^{-2}$ mm / year, leading to 6.3% of the highlands experiencing upwelling (Figure 6b). This solution is obtained using a fairly large recharge band from $-45°$ to $45°$, however, the numeric model is less sensitive to recharge distribution than the analytic model. This is due to the irregular geometry of the shoreline and shortened travel paths to standing bodies of water such as Argyre and Hellas basins as well as Valles Marineris. If the recharge band is reduced to $-30°$ to $30°$, the same 6.3% upwelling is observed with only 5μm/yr additional recharge. The calculated r/K remains on the order of $\sim 10^{-5}$. This is insensitive to any reasonable

257 assumptions regarding recharge distribution and therefore can be used to estimate plausible values of r for any preferred
258 value of K.

4. Discussion

260 Our results show that a groundwater aquifer beneath the highlands requires very low recharge values to avoid
261 groundwater upwelling occurring outside areas suggested by observational evidence. We show that the plausible
262 steady-state recharge increases linearly with the assumed mean hydraulic conductivity of the aquifer. As such, plausible
263 recharge values for any preferred hydraulic conductivity can be estimated as $r \sim 10^{-5} K$. This relationship is evident
264 from the analytic solutions (equation 8) and confirmed by numerical models of varying complexity. Whereas the
265 geometry of the shorelines has a small effect on the overall magnitude of recharge, Mars' planetary scale topography
266 requires upwelling to occur first in Arabia Terra as recharge increases, in agreement with previous work (Andrews-
267 Hanna et al., 2007). If groundwater is assumed to be at or near the surface primarily in Arabia Terra and the chosen K
268 value is held constant, the range of plausible recharge fluxes varies by less than one order of magnitude (Figure 6d).
269 This is consequential because physically informed hydraulic conductivity estimates can be made. Here, we employed
270 a value that is commonly used in Mars groundwater studies (Hanna and Phillips, 2005; Andrews-Hanna et al., 2010;
271 Horvath and Andrews-Hanna, 2017).

272 Previous global groundwater studies estimate recharge fluxes from $\sim 10^{-2}$ mm/yr (Andrews-Hanna et al., 2007) to
273 $\sim 10^{-1}$ m/yr (Andrews-Hanna and Lewis, 2011) for comparable mean hydraulic conductivities, see SI Section S4.1.
274 These estimates are consistent with our results and suggest that they are not strongly dependent on model assumptions.
275 This provides confidence in our methods, given that our model is fundamentally different from any previously published
276 global-scale Martian groundwater model. In previous work, there were no numerical mechanisms to create a complex
277 domain that allowed for standing water and resultant shorelines. Any water that breached the topography was assumed
278 to evaporate and then redistributed across the recharge band (Andrews-Hanna et al., 2007). In doing so, choosing the
279 initial level of the hydraulic head determines the hydraulic head gradients, and the initial hydraulic head gradients
280 control groundwater flux rates out of topographically low areas. The recharge then becomes a dynamic variable of
281 the initial condition rather than an independent parameter space. This modeling method also creates a model that
282 will iterate to steady state unless some method of perturbation is evoked, such as secular water loss. Previous global
283 scale models are essentially the extreme end member of this work in which there is no standing water. Despite all the
284 differences in the model methods and parameterizations, the estimated steady recharge fluxes predicted by previous
285 global models that do not include standing water is $0.01 mm/yr$ while our model prediction is $\sim 0.03 mm/yr$ (Figure
286 6b).

287 We suggest that low values of acceptable mean recharge are due to the large surface area, A_s, of the aquifer relative
288 to its small cross-sectional area, A_x. This geometric control can be understood by a volume balance over a spherical cap
289 aquifer at steady state. The total rate of recharge is $Q_r = A_s r$ and the total discharge out of the aquifer is $Q_d = A_x q_\theta$,
290 where q_θ is volumetric flux from Darcy's law. Total volume balance requires that $Q_d = Q_r$, so that

$$\frac{r}{K} = \frac{A_x}{A_s} q_\theta \sim \frac{d\Delta h}{R^2} \sim 10^{-5}, \tag{10}$$

291 where $R \sim 10^6$ m is the radius of Mars, $d \sim 10^4 m$ is the thickness of the aquifer and $\Delta h \sim 10^3$ m is the elevation
292 change of the groundwater table across the aquifer. Here, we have approximated $A_s \sim R^2$ and $A_x \sim R$ and Darcy's law
293 as $q_\theta \sim K\Delta h/R$. This simple estimate is identical to the r/K ratio obtained from the analytic solution and computed
294 from the numerical models (see SI Section S1). It is noteworthy that four methods produced equivalent r/K values.
295 The simple back of the envelope calculation in equation 10, the analytic solutions in equation 9, our complex numerical
296 model, and previous work by Andrews-Hanna et al. (2007;2010, Appendix C) produce nearly identical results.

297 Although previous work has computed specific recharge values for specific model parameters, our contribution
298 demonstrates the linear relation between r and K that allows estimates of plausible steady recharge for any assumed
299 value of K. This is valuable precisely because K is highly uncertain and the linear relationship allows for the
300 investigation of different scenarios. For example, consider a steady hydrologic cycle in which a significant fraction
301 of precipitation infiltrates and recharges the aquifer. To align with published precipitation estimates, it would require
302 an increase in our model's recharge by nearly two orders of magnitude (Figure 6d). The linear relation between r
303 and K would thus require a two order of magnitude increase in the mean conductivity of the aquifer to keep upwelling
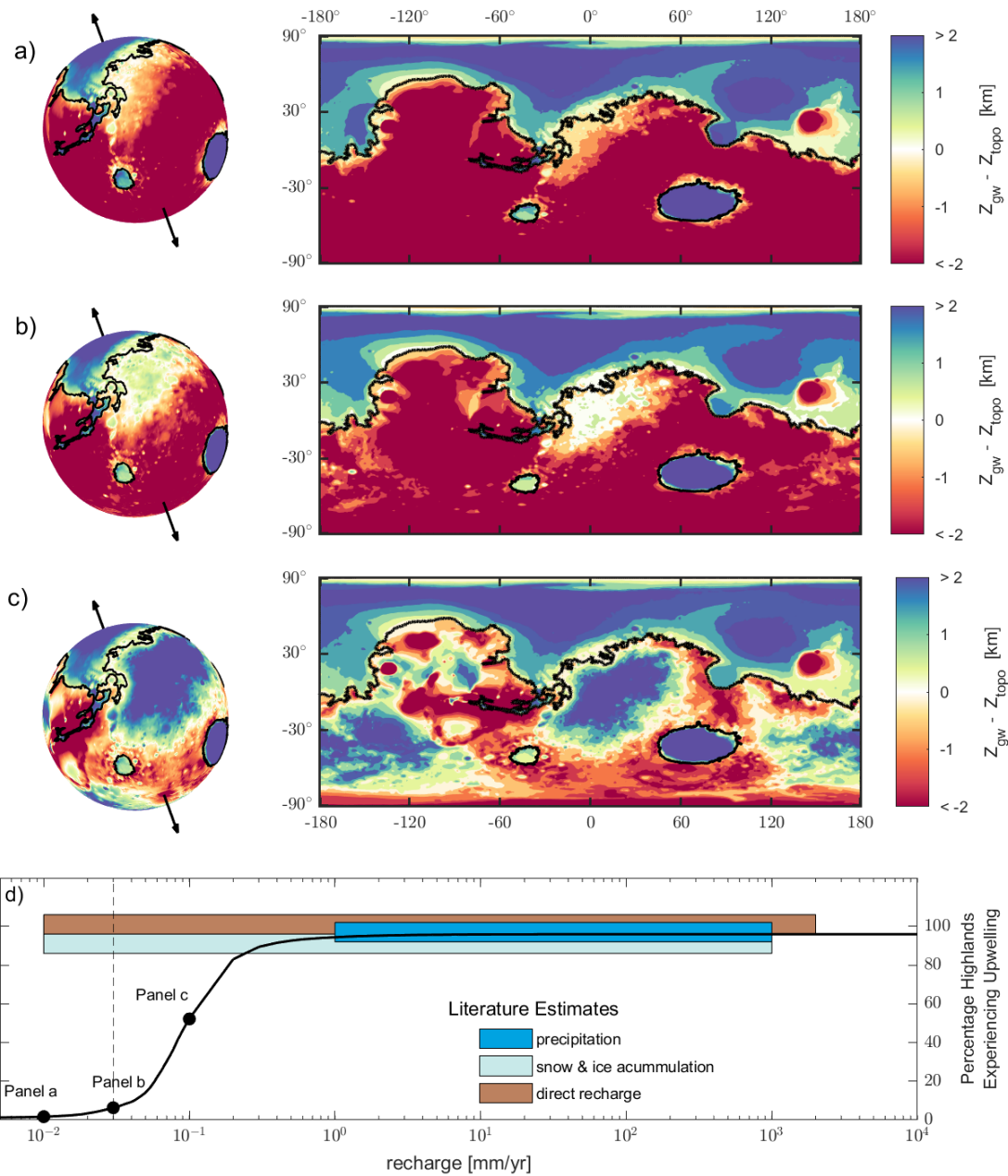
Figure 6: Groundwater upwelling as a function of recharge for an aquifer bounded by the Arabia shoreline and equal elevation shorelines in Hellas and Argyre. Recharge, r, is evenly distributed between -45° and 45° and $K = 10^{-7}$ m/s. a) $r = 1 \cdot 10^{-2}$ mm/yr. b) $r = 3 \cdot 10^{-2}$ mm/yr. c) $r = 1 \cdot 10^{-1}$ mm/yr. d) Percentage of the southern highlands area experiencing groundwater upwelling as function of recharge with estimates of water availability (Stucky de Quay et al., 2021). The vertical dashed line represents the preferred value of plausible recharge represented in panel b.

restricted to Arabia Terra. This would require the entire 10 km thick aquifer to have the conductivity of karstic limestone (Freeze and Cherry, 1977).

While local variations in K by several orders of magnitude are not unusual, the K in our equations is the average over the entire aquifer. This average includes rapid decay of the conductivity with depth (Shadab et al., 2023). As such, it is unlikely that the mean K of the aquifer could increase to the value of 10^{-5} m/s, required to make the recharge

comparable with precipitation estimates of more than 1 mm/yr. If conductivity is lower than assumed here and in previous work (Clifford, 1993; Clifford and Parker, 2001; Hanna and Phillips, 2005), the r/K-relation requires that groundwater recharge in a steady hydrologic cycle is orders of magnitude less than published precipitation estimates (Kamada et al., 2020; Wordsworth et al., 2015). It should be noted that the precipitation estimates are spatially variable. Our work represents both spatially and temporally averaged rates, and this may result in higher recharge values locally. However, the order of magnitude difference between the precipitation estimates and groundwater recharge can only be explained by a few possible mechanisms.

All of the above considerations assume a steady hydrological system because the model presented is at steady state. However, Mars' hydrological activity is believed to occur during short climatic excursions that produce favorable conditions for precipitation (Grotzinger et al., 2014; Wordsworth et al., 2015; Stucky de Quay et al., 2021). In this context, our recharge estimates should be interpreted as average over hydrologically active and inactive periods. As such, the recharge during active periods would almost certainly exceed steady-state values. The large discrepancy between the steady-state recharge fluxes found here and published estimates of precipitation can likely be explained by a combination of several processes.

The simplest way to explain the order-of-magnitude discrepancy between the published precipitation estimates and this work is that both are correct. This would require most precipitation to form runoff rather than recharge the highlands aquifer. It is likely that a combination of a run-off driven system and a delayed transient aquifer response to recharge is the most likely scenario capable of producing published precipitation estimates with low enough recharge fluxes to produced the observed geology.

The transient response of the groundwater table to individual ephemeral precipitation events would depend on the depth of the groundwater table below topography when the recharge event begins, as well as the duration and intensity of recharge. If the transient response time of the aquifer to rise and breach topography is longer than the timescale of climate excursions producing higher recharge values, the groundwater table may not breach the surface before the excursion ends and the recharge declines. The transient aquifer response will be examined in future work and will have implications for constraining the intensity and longevity of climatic events capable of producing recharge.

Lastly, another consideration would be Mars' total water budget. If the Mars GEL (global equivalent layer) were sufficiently low, the evaporative loss would deplete the sources of precipitation and prevent recharge from continuing. In our model simulations with the Arabia Terra shoreline and our preferred recharge value of $3 \cdot 10^{-2}$ mm/yr, the total volume of water contained in the Mars southern highlands aquifer is $\sim$ 670 m GEL , see SI Section S4.2 for calculation. This is a median value compared to values in the literature that range from 100 to 1500 m (e.g., Scheller et al., 2021). However, if there was a significantly limited water budget or a substantial portion of the GEL was not involved in subsurface-surface-atmosphere exchange during the hydrologically active period, a lack of available water as a precipitation source could limit recharge.

Future work will focus on the transient response of groundwater table as well as the conditions required for groundwater connection between the large basins. Each work will require modeling with a dynamic domain for which the algorithm was created in this work. As ocean and basin shorelines move in response to climatically forced evaporation and precipitation, these groundwater-topography interactions must be accounted for. To do so, the governing equation must be modified, and this requires an estimate of r/K (Bresciani et al., 2014, 2016).

5. Conclusions

Our analytical and numerical solutions for the Martian highlands aquifer show that the elevation of the groundwater table is controlled by the ratio of the mean recharge to the mean hydraulic conductivity of the aquifer. This ratio is a function of the geometry associated with the planetary dichotomy. It has implications for constraining the early Martian climate because it allows for estimates of plausible recharge fluxes given any preferred values for aquifer conductivity. For commonly assumed conductivities of $\sim 10^{-7}$ m/s (permeability $\sim 10^{-14}$ m^2) the mean groundwater recharge on the highlands is $\sim 10^{-2}$ mm/yr. This value is at the low end of previously proposed estimates and two orders of magnitude below estimates of precipitation. If the hydrologic cycle is at steady-state and published precipitation estimates are correct, then our groundwater models imply that some combination of three possible factors can create low recharge with higher values of precipitation. These possibilities include that most precipitation forms runoff, the transient response of the aquifer to recharge is sufficiently slow that widespread upwelling did not occur prior to the cessation of the recharge event, and/or the total water available as surface sources of precipitation are exhausted prior to widespread upwelling.

Acknowledgements

M.A.H. acknowledges support from NASA Emerging World Grant number $18-EW18\_2-0027$. E.H. acknowledges support from the Gale White Fellowship from the University of Texas Institute for Geophysics (UTIG), the Center for Planetary Systems Habitability (CPSH) through the Student Research Award in Planetary Habitability. M.A.S. acknowledges support from the University of Texas Institute for Geophysics (UTIG) through Graduate Student Fellowship, and the Center for Planetary Systems Habitability (CPSH) through the Student Research Award in Planetary Habitability. This is UTIG Contribution #XXXX and CPSH Contribution #XXXX.

Two anonymous reviewers are thanked for insightful comments that significantly improved the quality of this work. Dr. Elizabeth Rampe is thanked for editorial handling. The authors also thank Dr. Edwin Kite, Dr. Jack Mustard, Dr. Francesco Salese, and Dr. David Horvath for helpful discussions.

References

D. E. Smith, M. T. Zuber, S. C. Solomon, R. J. Phillips, J. W. Head, J. B. Garvin, W. B. Banerdt, D. O. Muhleman, G. H. Pettengill, G. A. Neumann, et al., The global topography of mars and implications for surface evolution, science 284 (1999) 1495–1503.

M. H. Carr, Mars: A water-rich planet?, Icarus 68 (1986) 187–216.

S. Clifford, A model for the hydrologic and climatic behavior of water on mars, Journal of Geophysical Research: Planets 98 (1993) 10973–11016.

H. Frey, Ages of very large impact basins on Mars: Implications for the late heavy bombardment in the inner solar system, Geophysical Research Letters 35 (2008) 1–4.

S. Werner, The early martian evolution—constraints from basin formation ages, Icarus 195 (2008) 45–60.

D. J. Milton, Water and processes of degradation in the martian landscape, Journal of Geophysical Research 78 (1973) 4037–4047.

J. M. Goldspiel, S. W. Squyres, Ancient aqueous sedimentation on mars, Icarus 89 (1991) 392–410.

M. H. Carr, Water on mars, New York: Oxford University Press (1996).

B. M. Hynek, R. J. Phillips, Evidence for extensive denudation of the martian highlands, Geology 29 (2001) 407–410.

J. F. Mustard, S. L. Murchie, S. Pelkey, B. Ehlmann, R. Milliken, J. A. Grant, J.-P. Bibring, F. Poulet, J. Bishop, E. N. Dobrea, et al., Hydrated silicate minerals on mars observed by the mars reconnaissance orbiter crism instrument, Nature 454 (2008) 305–309.

B. L. Ehlmann, J. F. Mustard, G. A. Swayze, R. N. Clark, J. L. Bishop, F. Poulet, D. J. Des Marais, L. H. Roach, R. E. Milliken, J. J. Wray, et al., Identification of hydrated silicate minerals on mars using mro-crism: Geologic context near nili fossae and implications for aqueous alteration, Journal of Geophysical Research: Planets 114 (2009).

J. Carter, F. Poulet, J.-P. Bibring, N. Mangold, S. Murchie, Hydrous minerals on mars as seen by the crism and omega imaging spectrometers: Updated global view, Journal of Geophysical Research: Planets 118 (2013) 831–858.

N. A. Cabrol, E. A. Grin, Distribution, classification, and ages of martian impact crater lakes, Icarus 142 (1999) 160–172.

C. I. Fassett, J. W. Head III, Valley network-fed, open-basin lakes on mars: Distribution and implications for noachian surface and subsurface hydrology, Icarus 198 (2008) 37–56.

G. Di Achille, B. M. Hynek, Ancient ocean on mars supported by global distribution of deltas and valleys, Nature Geoscience 3 (2010) 459–463.

T. Parker, S. Clifford, W. Banerdt, Argyre planitia and the mars global hydrologic cycle, in: Lunar and Planetary Science Conference, 2000, p. 2033.

S. A. Wilson, J. M. Moore, A. D. Howard, D. E. Wilhelms, Evidence for ancient lakes in the hellas region, Lakes on Mars (2010) 195–222.

J. Dohm, T. Hare, S. Robbins, J.-P. Williams, R. Soare, M. R. El-Maarry, S. Conway, D. L. Buczkowski, J. S. Kargel, M. E. Banks, et al., Geological and hydrological histories of the argyre province, mars, Icarus 253 (2015) 66–98.

H. Hiesinger, J. W. Head, Topography and morphology of the argyre basin, mars: implications for its geologic and hydrologic history, Planetary and Space Science 50 (2002) 939–981.

H. I. Hargitai, V. C. Gulick, N. H. Glines, Paleolakes of northeast hellas: Precipitation, groundwater-fed, and fluvial lakes in the navua–hadriacus–ausonia region, mars, Astrobiology 18 (2018) 1435–1459.

J. Zhao, L. Xiao, T. D. Glotch, Paleolakes in the northwest hellas region, mars: Implications for the regional geologic history and paleoclimate, Journal of Geophysical Research: Planets 125 (2020) e2019JE006196.

T. Parker, S. Saunders, D. Schneeberger, Transitional morphology in west deuteronilus mensae, mars: Implications for modification of the lowland/upland boundary, Icarus 82 (1989) 111–145.

T. Parker, D. Gorsline, R. Saunders, D. C. Pieri, D. M. Schneeberger, Coastal geomorphology of the Martian northern plains, Journal of Geophysical Research 98 (1993) 11061–11078.

M. H. Carr, J. W. Head, Oceans on Mars: An assessment of the observational evidence and possible fate, Journal of Geophysical Research E: Planets 108 (2003) 1–28.

Andrews-Hanna, R. J. Phillips, M. T. Zuber, Meridiani Planum and the global hydrology of Mars, Nature 446 (2007) 163–166.

F. Salese, M. Pondrelli, A. Neeseman, G. Schmidt, G. G. Ori, Geological evidence of planet-wide groundwater system on mars, Journal of Geophysical Research: Planets 124 (2019) 374–395.

P. R. Christensen, J. Bandfield, R. Clark, K. Edgett, V. Hamilton, T. Hoefen, H. Kieffer, R. Kuzmin, M. Lane, M. Malin, et al., Detection of crystalline hematite mineralization on mars by the thermal emission spectrometer: Evidence for near-surface water, Journal of Geophysical Research: Planets 105 (2000) 9623–9642.

M. Golombek, J. A. Grant, T. Parker, D. Kass, J. Crisp, S. W. Squyres, A. Haldemann, M. Adler, W. Lee, N. Bridges, et al., Selection of the mars exploration rover landing sites, Journal of Geophysical Research: Planets 108 (2003).

S. W. Squyres, J. P. Grotzinger, R. E. Arvidson, J. F. Bell III, W. Calvin, P. R. Christensen, B. C. Clark, J. Crisp, W. H. Farrand, K. E. Herkenhoff, et al., In situ evidence for an ancient aqueous environment at meridiani planum, mars, science 306 (2004) 1709–1714.

Limited Recharge of the Southern Highlands Aquifer on Early Mars

419 S. M. McLennan, J. Bell Iii, W. Calvin, P. Christensen, B. d. Clark, P. De Souza, J. Farmer, W. Farrand, D. Fike, R. Gellert, et al., Provenance and
420   diagenesis of the evaporite-bearing burns formation, meridiani planum, mars, Earth and Planetary Science Letters 240 (2005) 95–121.
421 J. P. Grotzinger, R. Arvidson, J. Bell Iii, W. Calvin, B. Clark, D. Fike, M. Golombek, R. Greeley, A. Haldemann, K. E. Herkenhoff, et al., Stratigraphy
422   and sedimentology of a dry to wet eolian depositional system, burns formation, meridiani planum, mars, Earth and Planetary Science Letters
423   240 (2005) 11–72.
424 J.-P. Bibring, R. Arvidson, A. Gendrin, B. Gondet, Y. Langevin, S. Le Mouelic, N. Mangold, R. Morris, J. Mustard, F. Poulet, et al., Coupled ferric
425   oxides and sulfates on the martian surface, science 317 (2007) 1206–1210.
426 M. C. Malin, K. S. Edgett, Oceans or seas in the martian northern lowlands: High resolution imaging tests of proposed coastlines, Geophysical
427   Research Letters 26 (1999) 3049–3052.
428 S. F. Sholes, D. R. Montgomery, D. C. Catling, Quantitative high-resolution reexamination of a hypothesized ocean shoreline in cydonia mensae
429   on mars, Journal of Geophysical Research: Planets 124 (2019) 316–336.
430 S. F. Sholes, Z. I. Dickeson, D. R. Montgomery, D. C. Catling, Where are mars' hypothesized ocean shorelines? large lateral and topographic offsets
431   between different versions of paleoshoreline maps, Journal of Geophysical Research: Planets 126 (2021) e2020JE006486.
432 S. F. Sholes, F. Rivera-Hernández, Constraints on the uncertainty, timing, and magnitude of potential mars oceans from topographic deformation
433   models, Icarus 378 (2022) 114934.
434 J. Perron, J. Mitrovica, M. Manga, I. Matsuyama, M. Richards, Evidence for an ancient martian ocean in the topography of deformed shorelines,
435   Nature 447 (2007) 840–843.
436 R. I. Citron, M. Manga, D. J. Hemingway, Timing of oceans on mars from shoreline deformation, Nature 555 (2018) 643–646.
437 N.-H. Chan, J. T. Perron, J. X. Mitrovica, N. A. Gomez, New evidence of an ancient martian ocean from the global distribution of valley networks,
438   Journal of Geophysical Research: Planets 123 (2018) 2138–2150.
439 B. M. Hynek, M. Beach, M. R. Hoke, Updated global map of martian valley networks and implications for climate and hydrologic processes, Journal
440   of Geophysical Research: Planets 115 (2010).
441 J. Davis, M. Balme, P. Grindrod, R. Williams, S. Gupta, Extensive noachian fluvial systems in arabia terra: Implications for early martian climate,
442   Geology 44 (2016) 847–850.
443 J. M. Davis, S. Gupta, M. Balme, P. M. Grindrod, P. Fawdon, Z. I. Dickeson, R. M. Williams, A diverse array of fluvial depositional systems in
444   arabia terra: Evidence for mid-noachian to early hesperian rivers on mars, Journal of Geophysical Research: Planets 124 (2019) 1913–1934.
445 R. D. Wordsworth, L. Kerber, R. T. Pierrehumbert, F. Forget, J. W. Head, Comparison of "warm and wet" and "cold and icy" scenarios for early
446   Mars in a 3-D climate model, Journal of Geophysical Research: Planets 120 (2015) 1201–1219.
447 J. L. Fastook, J. W. Head, Glaciation in the late noachian icy highlands: Ice accumulation, distribution, flow rates, basal melting, and top-down
448   melting rates and patterns, Planetary and Space Science 106 (2015) 82–98.
449 P. von Paris, A. Petau, J. Grenfell, E. Hauber, D. Breuer, R. Jaumann, H. Rauer, D. Tirsch, Estimating precipitation on early mars using a radiative-
450   convective model of the atmosphere and comparison with inferred runoff from geomorphology, Planetary and Space Science 105 (2015) 133–147.
451 A. Kamada, T. Kuroda, Y. Kasaba, N. Terada, H. Nakagawa, K. Toriumi, A coupled atmosphere–hydrosphere global climate model of early mars:
452   A 'cool and wet' scenario for the formation of water channels, Icarus 338 (2020) 113567.
453 R. M. Ramirez, R. A. Craddock, T. Usui, Climate simulations of early mars with estimated precipitation, runoff, and erosion rates, Journal of
454   Geophysical Research: Planets 125 (2020) e2019JE006160.
455 M. R. Hoke, B. M. Hynek, G. E. Tucker, Formation timescales of large martian valley networks, Earth and Planetary Science Letters 312 (2011)
456   1–12.
457 K. P. Harrison, R. E. Grimm, Regionally compartmented groundwater flow on Mars, Journal of Geophysical Research E: Planets 114 (2009).
458 Andrews-Hanna, M. T. Zuber, R. E. Arvidson, S. M. Wiseman, Early Mars hydrology: Meridiani playa deposits and the sedimentary record of
459   Arabia Terra, Journal of Geophysical Research E: Planets 115 (2010) 1–22.
460 W. Luo, B. Grudzinski, D. Pederson, Estimating hydraulic conductivity for the martian subsurface based on drainage patterns—a case study in the
461   mare tyrrhenum quadrangle, Geomorphology 125 (2011) 414–420.
462 D. G. Horvath, J. C. Andrews-Hanna, Reconstructing the past climate at gale crater, mars, from hydrological modeling of late-stage lakes,
463   Geophysical Research Letters 44 (2017) 8196–8204.
464 S. Clifford, A model for the hydrologic and climatic behavior of water on Mars, Journal of Geophysical Research 98 (1993) 10973–11016.
465 Hanna, R. J. Phillips, Hydrological modeling of the Martian crust with application to the pressurization of aquifers, Journal of Geophysical Research
466   E: Planets 110 (2005) 1–19.
467 W. Luo, A. Howard, Computer simulation of the role of groundwater seepage in forming Martian valley networks, Journal of Geophysical Research
468   113 (2008) E05002.
469 J. Dupuit, Etudes théoriques et pratiques sur le mouvement des eaux dans les canaux découverts et àtravers les terrains perméable, 2nd ed., Dunod,
470   Paris, 1863.
471 P. Forchheimer, Wasserbewegung durch Boden, Zeitschrift des Vereins Deutscher Ingenieure 45 (1901) 1782–1788.
472 J. Boussinesq, Théorie Analytique de la Chaleur, Gauthier-Villars, Paris, 1903.
473 P. A. Troch, A. Berne, P. Bogaart, C. Harman, A. G. Hilberts, S. W. Lyon, C. Paniconi, V. R. Pauwels, D. E. Rupp, J. S. Selker, A. J. Teuling,
474   R. Uijlenhoet, N. E. Verhoest, The importance of hydraulic groundwater theory in catchment hydrology: The legacy of Wilfried Brutsaert and
475   Jean-Yves Parlange, Water Resources Research 49 (2013) 5099–5116.
476 Andrews-Hanna, Lewis, Early Mars hydrology: 2. Hydrological evolution in the Noachian and Hesperian epochs, Journal of Geophysical Research
477   E: Planets 116 (2011) 1–20.
478 M. A. Shadab, E. Hiatt, M. Hesse, Estimates of martian mean recharge rates from analytic groundwater models, LPI Contributions 2678 (2022)
479   1775.
480 R. LeVeque, Numerical Methods for Conservation Laws, Birkhaeuser Verlag, 1992.

Limited Recharge of the Southern Highlands Aquifer on Early Mars

[481] M. A. Shadab, M. Hesse, A hyperbolic-elliptic model and conservative numerical method for gravity-dominated variably-saturated groundwater flow, arXiv preprint arXiv:2210.04724 (2022).

[483] G. Stucky de Quay, T. A. Goudge, E. S. Kite, C. I. Fassett, S. D. Guzewich, Limits on runoff episode duration for early mars: Integrating lake hydrology and climate models, Geophysical Research Letters 48 (2021) e2021GL093523.

[485] R. A. Freeze, J. A. Cherry, Groundwater (1977).

[486] M. A. Shadab, E. Hiatt, M. Hesse, Investigating groundwater dynamics and residence times on early mars using unconfined aquifer model with vertical heterogeneity, LPI Contributions (2023) 1736.

[488] S. Clifford, T. Parker, The evolution of the martian hydrosphere: Implications for the fate of a primordial ocean and the current state of the northern plains, Icarus 154 (2001) 40–79.

[490] J. P. Grotzinger, D. Y. Sumner, L. Kah, K. Stack, S. Gupta, L. Edgar, D. Rubin, K. Lewis, J. Schieber, N. Mangold, et al., A habitable fluvio-lacustrine environment at yellowknife bay, gale crater, mars, Science 343 (2014) 1242777.

[492] E. Scheller, B. Ehlmann, R. Hu, D. Adams, Y. Yung, Long-term drying of mars by sequestration of ocean-scale volumes of water in the crust, Science 372 (2021) 56–62.

[494] E. Bresciani, P. Davy, J.-R. de Dreuzy, Is the dupuit assumption suitable for predicting the groundwater seepage area in hillslopes?, Water Resources Research 50 (2014) 2394–2406.

[496] E. Bresciani, P. Goderniaux, O. Batelaan, Hydrogeological controls of water table-land surface interactions, Geophysical Research Letters 43 (2016) 9653–9661.

Declaration of interests

☒ The authors declare that they have no known competing financial interests or personal relationships that could have appeared to influence the work reported in this paper.

☐ The authors declare the following financial interests/personal relationships which may be considered as potential competing interests: